ORIGINAL PAPER

Microstructural, dielectric, and transport properties of proton-conducting solid polymer electrolyte for battery applications

Shreedatta Hegde [1] · V. Ravindrachary [1] · S. D. Praveena [2] · Ismayil [3] · B. Guruswamy [1] · Rohan N. Sagar [1]

Abstract

Poly (vinyl alcohol) (PVA) complexed with ammonium chloride (NH_4Cl) solid polymer electrolyte films was prepared using solution casting technique. Complexation of dopant with polymer was studied using Fourier transform infrared spectroscopy (FTIR). X-ray diffraction (XRD) results reflect that degree of crystallinity of the polymer increases with doping level. Surface morphology and topology of the electrolyte were studied using Scanning electron microscopy (SEM) and atomic force microscopy (AFM). Thermogravimetric analysis (TGA) results accounts for the increase of thermal stability of PVA due to the incorporation of NH_4Cl. Impedance analysis was carried out to understand relaxation phenomena of polymer electrolyte. Dielectric studies revealed that the mobility of charge carriers follows non-Debye nature of ionic relaxation. Electrical studies reveal that proton conduction occurs in this polymer electrolyte through Grotthus mechanism and maximum conductivity of the polymer electrolyte (7.5 wt% NH_4Cl/PVA) has been observed to be 1.81×10^{-3} S/cm at 353 K. Transport parameters have been determined using Wagner's polarization technique. The observed highest conductivity of polymer electrolyte indicates utilizing this electrolyte for the fabrication of proton battery applications, and accordingly, the cell parameters have been measured.

Keywords Solid polymer electrolyte · PVA · NH_4Cl · Ionic conductivity · Transport property · Proton battery

Introduction

In recent years, the solid polymer electrolytes (SPE) have fascinated the researchers due to their potential applicability in the fabrication of solid-state devices. These extensive applications of SPE are mainly due to their good mechanical properties, ease of fabrication into thin films and their ability to form good electrode/electrolyte contact. Compared to gel/liquid electrolytes, advantages of SPEs are flexibility, lightweight, high ionic conductivity, high-energy density, leak proof, solvent-free condition, wide electrochemical stability and processability [1, 2]. Generally, the SPEs are prepared by doping a polymer such as poly (methyl methacrylate) (PMMA), polyethylene oxide (PEO), polyacrylonitrile (PAN) and poly (vinyl alcohol) (PVA) etc. with a salt of low lattice energy. It is known that change in the properties of doped polymer depends on nature of the host polymer, nature and type of dopant and the way in which the dopant interacts with host polymer [3]. Over the years, the efforts are made to improve thermal, mechanical as well as conducting properties of SPE using various approaches such as polymer blending, doping an inorganic salt or filler, addition of plasticizer etc. In particular, the research and development efforts have been strongly stimulated by the fabrication of rechargeable lithium ion batteries using SPE [4]. The disadvantages of these batteries are their high cost, maintenance of lithium electrodes and safety issues along with high electrochemical stability window of about ~ 4 V. An alternative to lithium-ion batteries is hydrogen ion (H^+) conducting proton batteries. Here, the proton is of smaller size; it intercalates in many host matrixes

✉ V. Ravindrachary
vravi2000@yahoo.com

1 Department of Physics, Mangalore University, Mangalagangotri, Konaje 574199, India

2 Department of Physics, K. V. G. College of Engineering, Kurunjibhag, Sullia 574327, India

3 Department of Physics, Manipal Institute of Technology, Manipal Academy of Higher Education, Manipal 576104, India

which increases its mobility and hence affects the conductivity. The electrochemical stability window for proton batteries is ~ 1 V which offers advantage on the basis of energy-density consideration, and proton batteries can be used in low energy density battery applications [5]. Hence, the proton-conducting SPEs have become an attractive material for study because of their wide range of applications in many technological areas such as fuel cells, super capacitors, solid-state batteries and electro-chemical devices [6]. For a successful battery performance, the SPE must possess sufficient ionic conductivity. Various methods have been adopted to enhance conductivity of the polymer electrolyte such as thermal evaporation method, hot pressing method, solution casting method, flash evaporation method, pyrolysis, film blowing and sputtering etc. One of the simplest economical methods used to obtain SPE is to dissolve an inorganic salt within the polymer matrix by solution cast technique. From literature, it is clear that the proton-conducting polymer electrolytes are complexes of strong inorganic acid like HCl or ammonium salts with commercially available electron-donor polymers such as poly (acrylic acid) (PAA), PEO, PVA. However, proton-conducting polymer complex with inorganic acids suffers from chemical degradation and mechanical integrity making them unsuitable for practical applications [7]. So, the proton conducting SPE prepared by doping of ammonium salt to a polymer is more preferred.

Many researchers have reported that the ammonium salts such as NH_4Br, NH_4I, NH_4F and NH_4NO_3-doped PVA are very good proton donors. Similarly ammonium chloride (NH_4Cl) is a proton donor (crystalline in nature) and its incorporation into polymer matrix enhances proton conduction. In ammonium salt-doped polymer electrolytes, proton transfer takes place which is because of the motion of groups like NH_4^+, H^+, H_3O^+ which are used in fuel cells [8–10]. PVA is a semi-crystalline polymer with hydroxyl group attached to methane carbons which can be a source of hydrogen bonding. It is a low cost, nontoxic, water soluble synthetic polymer with high tensile strength and is used in biochemical as well as medical applications because of its compatibility with the living body. It also possesses high mechanical strength and excellent film-forming ability, dopant-dependent electrical and optical properties. It is known that the physical and chemical properties of PVA can be tuned by doping with metal salts. Since PVA is a polar polymer, the cation of the dopant coordinate with polar groups of the polymer and forms complex either in crystalline phase or amorphous phase of PVA and expected to change its structural, electrical, morphological and thermal properties [11].

Hence, the present work aims to study the NH_4Cl-doped PVA polymer electrolyte. The changes induced on structural, morphological, topological, thermal and electrical properties of the polymer by the dopant has been studied using various experimental techniques such as FTIR, XRD, SEM, AFM, TGA and electrical studies.

Experimental details

Sample preparation and characterization

The PVA in powder form (with an average molecular weight 1, 25,000) was obtained from M/s CDH (P) Ltd. Mumbai and NH_4Cl salt from M/s LOBA Chemie Mumbai. Pure PVA and NH_4Cl salt-doped PVA films were prepared by solution cast technique using double distilled water as solvent [10]. Thickness of the films was in the range of 0.08–0.10 mm. The films with 0.5, 1, 2.5, 5 and 7.5 wt% (M (wt%)) of dopant concentrations were prepared according to the relation

$$M = \frac{m_d}{m_p + m_d} \times 100 \qquad (1)$$

where m_d and m_p are the mass of dopant and polymer, respectively. The polymer electrolyte films are not stable for higher concentration (above 7.5 wt%) of NH_4Cl dopant, and hence, the study has been restricted to 7.5 wt% dopant concentration. FTIR spectra were recorded using SHIMADZU IR-Prestige-21 Fourier transform infrared spectrophotometer in the wavenumber range 400–4000 cm^{-1} to identify the possible chemical changes within the electrolyte. X-ray diffraction spectra were recorded using RIGAKU MINIFLEX-600 benchtop X-ray diffractometer with Cu-Kα radiation (wavelength 1.5406 Å) in the 2θ range 10–60° with a scanning speed of 1° per min and a step size of 0.02°. Surface morphology of polymer films has been studied using CARLZEISS scanning electron microscope. Here, the samples were gold coated using a sputter coater for 6 min before the imaging to minimize the sample charging effects due to electron beam. The surface topology was recorded on NANOSURF EZ2-Flex atomic force microscope. Thermal properties of the sample were studied using TGA in the temperature range of 30–600 °C at a scanning rate of 10 °C/min using Universal TA-SDT Q600 instrument. Electrical studies were carried out using Agilent 4294A Precision Impedance Analyzer in the frequency range 40 Hz–5 MHz. Relaxation behavior of polymer electrolytes has been studied using Cole-Cole plot in the same frequency range over which the electrical studies have been carried out. Transport and transient properties were studied according to Wagner's polarization technique using Keithley-236 source measure unit.

Preparation of anode, cathode electrodes and fabrication of proton battery

To prepare anode electrode, a mixture of zinc metal powder or zinc dust, $ZnSO_4 \cdot 7H_2O$ and graphite powder were taken in the weight ratio 3:1:1 and mixed homogeneously in a mortar. For cathode, lead oxide (PbO_2), vanadium pentoxide (V_2O_5), graphite powder and polymer electrolyte were taken in the

weight ratio 8:2:1:0.5 and then mixed in a mortar. The intention of adding graphite powder was to introduce electronic conductivity and the polymer electrolyte reduces electrode polarization [12]. The slurries of finely powdered anode and cathode mixtures were prepared using N-Methyl-2-pyrrolidone (NMP) solvent and coated the anode slurry on copper foil and cathode slurry on aluminum foil. These were dried completely and then the polymer electrolyte (with highest conductivity) is sandwiched between anode and cathode electrodes. Cathode (Al foil) acts as positive electrode and anode (Cu foil) acts as negative electrode. Then, the battery cell is allowed to stabilize in open circuit condition.

Results and discussion

Fourier transform infrared analysis

Observed FTIR spectra of pure PVA, pure NH_4Cl and NH_4Cl-doped PVA electrolyte films are given in Fig. 1 and the corresponding peak assignments are listed in Table 1. From Fig. 1, it is clear that for pure PVA, a broad band is observed at 3425 cm^{-1} and is assigned to O–H stretching vibrations of hydroxyl groups. Bands observed at 2928 cm^{-1} and 2853 cm^{-1} correspond to C–H asymmetric and C–H symmetric stretching vibrations. The observed band at 1733 cm^{-1} is assigned to C=O stretching vibrations and band at 1640 cm^{-1} corresponds to C=C group stretching vibrations. Bands appeared at 1438 cm^{-1} and 1378 cm^{-1} correspond to bending,

Fig. 1 FTIR spectra of pure PVA and NH_4Cl/PVA electrolyte films

wagging of CH_2 vibrations. A sharp band at 1089 cm^{-1} corresponds to C–O stretching of acetyl group present in PVA back bone and observed band at 790 cm^{-1} corresponds to C–H deformation [11]. For doped PVA films, the O–H band of pure PVA is shifted to 3287 cm^{-1} for 7.5 wt% of NH_4Cl concentration along with increase in intensity. The asymmetric and symmetric stretching vibrational bands of pure PVA are also shifted to 2922 cm^{-1} and 2846 cm^{-1} upon doping. The band corresponding to C=O group is shifted from 1733 to 1713 cm^{-1}. Other bands like bending and wagging of CH_2 vibrations are shifted to 1435 cm^{-1} and 1372 cm^{-1}. The band corresponding to acetyl group is shifted to 1091 cm^{-1}. C–H deformation of PVA is shifted to 843 cm^{-1} in the electrolytes. In addition to these changes in the IR bands of the electrolyte, a new band is also observed around 1251 cm^{-1} in the 0.5 wt%, which corresponds to C–H wagging and is shifted to 1261 cm^{-1} for 7.5 wt% dopant concentration [13]. All these changes in NH_4Cl-doped PVA electrolyte are the evidences for considerable interaction between dopant and polymer that lead to complex formation through inter and intramolecular hydrogen bonding. This interaction is thought to be with the hydroxyl group as well as C=O group of PVA. Hence, the appearance of new peak along with changes in existing peaks in FTIR spectra confirmed complexation between polymer and salt.

XRD studies

The observed X-ray diffractrogram for pure as well as NH_4Cl-doped PVA electrolyte films is shown in Fig. 2. For pure PVA figure shows that a relatively sharp and broad peak centered at $2\theta = 19.568°$ confirms the semicrystallinity of PVA [14]. In NH_4Cl-doped electrolytes, nature of the broad peak ($2\theta = 19.43°$) is unchanged and few sharp peaks appeared at $2\theta = 28.6°$ and $41.1°$. But these peaks do not exactly coincide with peaks of pure NH_4Cl which appeared at 23.1° and 40.3° in the literature [15]. With increase of dopant concentration, the intensity of these peaks increases and is shifted to lower angles, which indicate the increase of crystallinity of the electrolytes.

The degree of crystallinity (X_c) of the electrolytes is estimated from the ratios of areas under crystalline peaks and areas under amorphous peaks using the equation

$$X_c = \frac{A_c}{A_c + A_a} \times 100 \qquad (2)$$

where areas of sharp crystalline peaks and amorphous halos are indicated as A_c and A_a. Estimated crystallinity of the electrolytes is tabulated in Table 2 and it shows that crystallinity of the polymer increases with increase of dopant concentration. This enhancement in crystallinity is attributed to interaction of dopant with polymer as well as complex formation (as observed in FTIR study). The presence of these complexes
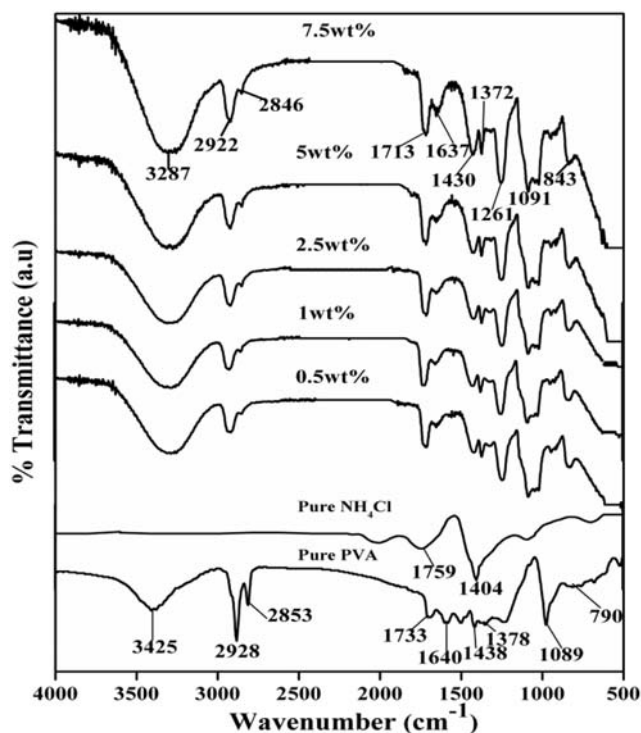
Table 1 FTIR peak assignments of pure PVA and 7.5 wt% NH$_4$Cl/PVA films

Wave numbers (cm^{-1})		Peak assignments
Pure PVA	7.5 wt% NH$_4$Cl-doped PVA	
3425	3287	O–H stretching vibration
2928	2922	C–H asymmetric stretching vibration
2853	2846	C–H symmetric stretching vibration
1733	1713	C=O stretching vibration
1640	1637	C=C stretching vibration
1438	1435	Bending of CH$_2$ vibration
1378	1372	Wagging of CH$_2$ vibration
–	1261	C–H wagging
1089	1091	C–O stretching
790	831	C–H deformation

affects the molecular mobility and increases the molecular ordering of the polymer. Here, dopant occupies the interstitial sites between polymer chains of amorphous phase and link them to hydrogen bonding. This hydrogen bonding increases with dopant concentration. At higher concentrations, it is expected that the dopant aggregates itself leading to a phase separation into polymer-rich phase and dopant-rich phase. These aggregates are represented in the form of average crystallite size (P) and the same has been determined using the Scherrer's equation [11]

$$P = \frac{k\lambda}{\delta} cos\theta \qquad (3)$$

where $k = 0.9$ is the constant and is related to shape of the crystal, the miller index of reflecting crystallographic planes
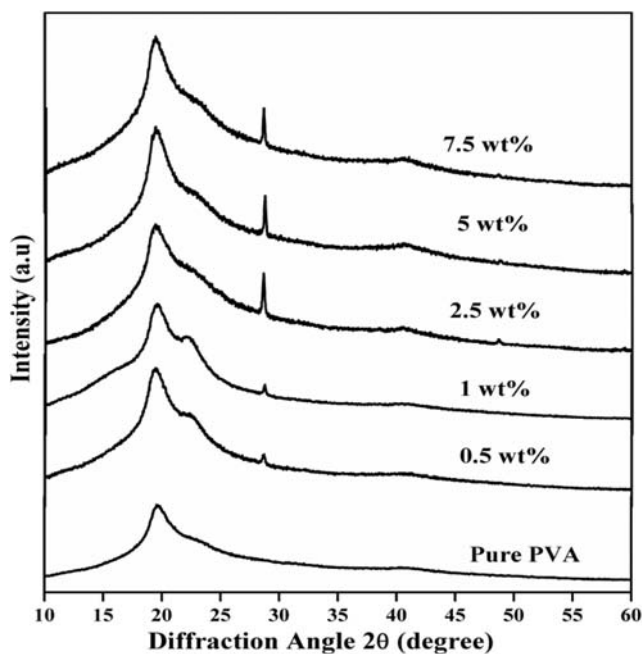
and also crystallite shape, δ is the full width at half maximum intensity of reflection in radians, θ is the Bragg's angle, $\lambda = 1.5406$ Å is the wavelength of X-ray radiation. The calculated average crystallite sizes are listed in Table 2. From the table, it is clear that the value of P increases with dopant concentration. To understand more about this variation, average inter crystallite separation (R_i) in the sample is determined using the equation [11]

$$R_i = \frac{5\lambda}{8sin\theta} \qquad (4)$$

The estimated R_i is tabulated in Table 2 and it shows that inter crystallite separation increases with increase of dopant concentration. From the above results, it is clear that the dopant NH$_4$Cl significantly modified the microstructure of the polymer PVA.

Scanning Electron microscopy and atomic force microscopy studies

Figure 3 a–c show the observed SEM micrographs of pure PVA (Fig. 3a), 2.5 wt% (Fig. 3b), and 7.5 wt% (Fig. 3c) NH$_4$Cl/PVA electrolytes. From the Fig. 3a, it is observed that SEM image of pure PVA exhibits a semicrystalline morphology such as the uniformly distributed small shiny areas (crystallites) in amorphous phase. After the addition of dopant, the shiny areas are observed in larger size and they appeared in large number (Fig. 3b). At higher dopant concentration, there is a strong tendency of aggregation of NH$_4$Cl particles within the polymer electrolytes and also formation of NH$_4$Cl particle clusters [16]. Figure 3 c shows that this cluster (aggregates) size increases with dopant concentration which indicates that the ammonium chloride particles are randomly dispersed on surface of the polymer. At higher dopant concentrations, these aggregates are reflected in the form of phase separation into polymer-rich phase and dopant-rich phase.

Fig. 2 XRD spectra of pure PVA and NH$_4$Cl/PVA electrolytes

Table 2 XRD result of pure PVA and NH$_4$Cl/PVA electrolytes

Sample (wt%) PVA + NH$_4$Cl	2θ	d-spacing (Å)	P (nm)	R$_i$ (Å)	% Crystallinity
0	19.568	4.5347	1.6743	5.6681	56
0.5	19.430	4.6794	1.9607	5.7083	59
	28.677	1.3758	1.9947	3.8880	
	41.158	2.1914	2.0643	2.7393	
1	19.535	5.5394	1.9989	5.6756	62
	29.417	3.7013	2.0370	3.7923	
	40.357	2.2331	1.2601	2.7913	
2.5	19.387	5.5813	2.0236	5.7185	69
	28.599	3.8048	2.0593	3.8984	
	40.496	1.8702	0.5709	2.7821	
5	19.354	5.5907	2.3066	5.7282	74
	28.669	3.7957	2.1214	3.8891	
	40.482	2.2264	2.1906	2.7831	
7.5	19.274	5.6137	2.3795	5.7517	78
	28.644	3.7990	2.1341	3.8924	
	40.30	2.7280	2.0966	2.7951	

Hence, morphology study showed phase segregation phenomenon in polymer electrolytes.

Figure 3 d–f portray three-dimensional topographs of pure PVA (Fig. 3d), 2.5 wt% (Fig. 3e), and 7.5 wt% (Fig. 3f) NH$_4$Cl-doped PVA electrolytes. Topograph of pure PVA consists of some sharp peaks and broad hump like structures which indicates semicrystalline nature of PVA as depicted in XRD and SEM results. In NH$_4$Cl-added PVA electrolytes (Fig. 3e), some pores appeared on the microstructure of the sample which facilitates the mobility of charge carriers [17]. The figure shows that the peaks become sharpen with increase of dopant concentration (Fig. 3f) and also surface roughness
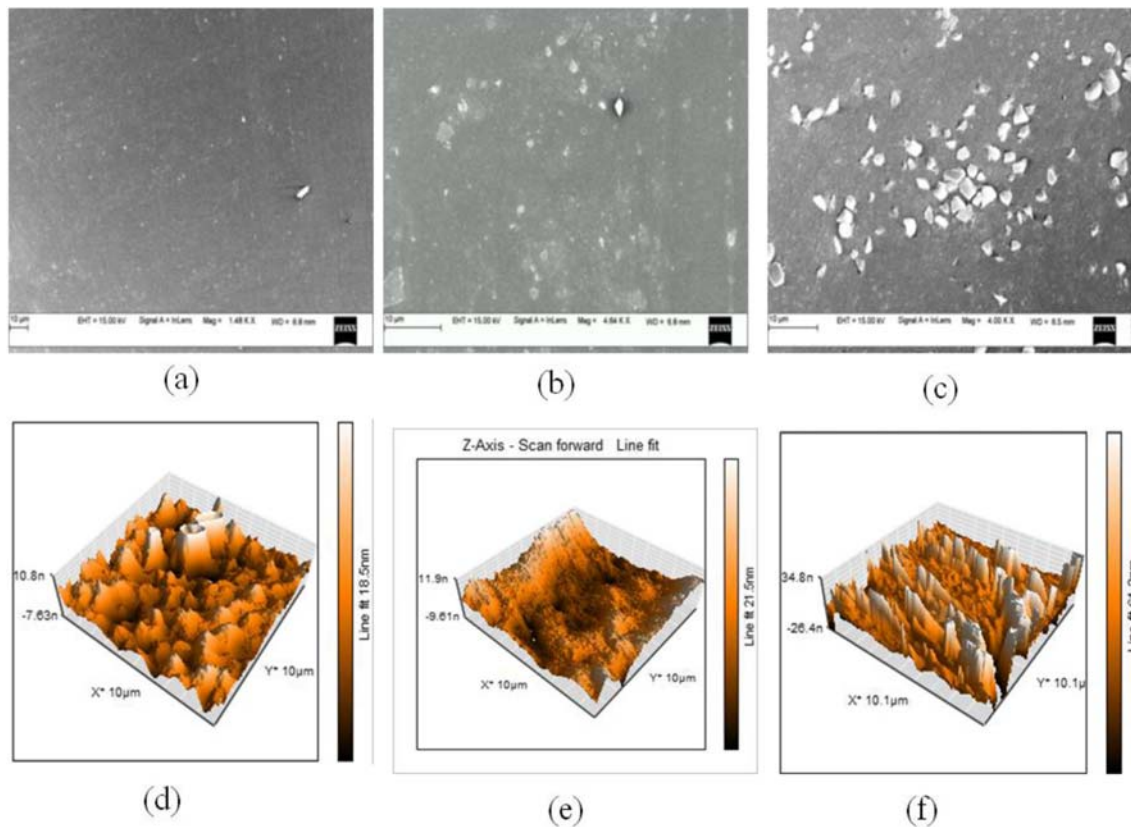

Fig. 3 **a–c** SEM images of pure PVA and NH$_4$Cl/PVA films, **d–f** AFM topographs of pure PVA and NH$_4$Cl-doped PVA films

Table 3 Roughness values of pure PVA and NH₄Cl/PVA electrolytes

Sample composition	Surface roughness	RMS roughness
Pure PVA	2.78 nm	3.92 nm
2.5 wt%	3.22 nm	3.97 nm
7.5 wt%	6.05 nm	10.80 nm

Table 4 Weight loss of pure PVA and NH₄Cl/PVA electrolytes at different temperatures

Doping level M (wt%)	Weight loss (wt%)				
	100 °C	200 °C	300 °C	400 °C	500 °C
0	5.57	7.08	16.72	72.54	98.99
0.5	4.95	7.8	19.58	67.98	95.01
1	3.38	8.46	25.64	62.87	96.92
2.5	5.94	10.06	32.98	60.31	91.83
5	4.98	11.33	45.37	59.67	87.67
7.5	5.94	13.57	38.06	58.43	82.28

has increased. This feature indicates that the dopant is not completely dissolved into the polymer; instead, it has deposited randomly on surface of the polymer. The topographs exhibit surface height variation of −7.63 to 10.8 nm (Fig. 3d), −9.61 to 11.9 nm (Fig. 3e) and −26.4 to 34.8 nm (Fig. 3f). The value of surface roughness and root mean square (RMS) roughness has been determined using NANOSURF software and is listed in Table 3. This study clearly suggests that the dopant NH₄Cl has dispersed on the surface of the polymer and the excess addition of dopant leads to the phase segregation.

Thermogravimetric analysis

Figure 4 a shows the observed TGA thermograph of pure and doped polymer films and the corresponding weight loss at different temperatures is given in Table 4. From the plot, it is evident that two major weight losses are observed in the temperature range of 90–150 °C and 300–452 °C for pure PVA which are attributed to evaporation of solvent as well as degradation of PVA by the dehydration reaction of polymer chain. For electrolyte films, first weight loss is observed around 60–130 °C (10%) that may be due to the evaporation of the absorbed water. Second weight loss observed around 210–460 °C temperature range (75%) represents the degradation temperature of PVA which is attributed to splitting of scission monomers and bonds in the polymeric backbone and loss of dopant due to thermal energy [18, 19].

Compared to pure PVA, thermal degradation in the electrolyte is shifted to higher temperatures (Table 4)

and the weight loss of the polymer electrolyte decreases with increase of dopant concentration in the region around 370–500 °C. Increase of degradation temperature is due to volume effects and complexation of dopant with polymer [20]. At temperatures greater than 520 °C, TGA curves level off. From all these changes, it is clear that thermal properties of the polymer are significantly modified with dopant concentration.

To understand the thermal decomposition of the polymer electrolyte further, activation energy has been determined using the integral equation of Coats and Redfern [21].

$$log\left[\frac{1-(1-\gamma)^{1-n}}{T^2}\right] = log\frac{R}{\Delta E}\left[1-\frac{2RT}{E_a}\right]-0.434\frac{E_a}{RT} \qquad (5)$$

where E_a is the activation energy in J/mol which is the least energy required to activate the molecules of polymer to undergo phase transition, T is the absolute temperature in Kelvin, R is the universal gas constant (8.3136 J/mol. K), n is the order of reaction and γ is the fractional weight loss at particular temperature which can be calculated using the following relation

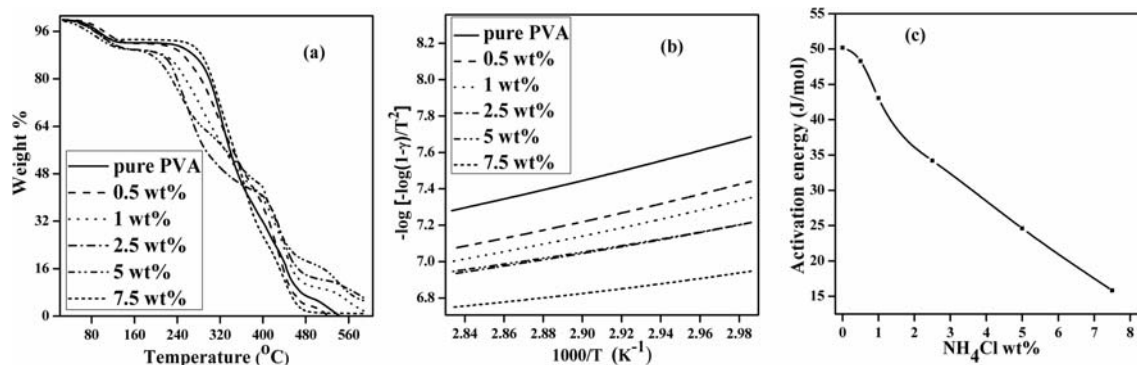$$\gamma = \frac{w_i - w_t}{w_i - w_f} \qquad (6)$$

Fig. 4 **a** TGA thermograph of pure PVA and NH₄Cl/PVA electrolytes. **b** Variation of $-log\left[\frac{-log(1-\gamma)}{T^2}\right]$ v/s reciprocal of absolute temperature. **c** Variation activation energy with dopant concentration

Here, w_i is the initial weight of the sample, w_t is the weight of the sample at given temperature and w_f is the final weight of the sample. For $n = 1$, Eq. (5) can be written as

$$log\left[\frac{-log(1-\gamma)}{T^2}\right] = log\frac{R}{\Delta E}\left[1-\frac{2RT}{E_a}\right]-0.434\frac{E_a}{RT} \quad (7)$$

By plotting $-log\left[\frac{-log(1-\gamma)}{T^2}\right]$ versus $\frac{1,000}{T}$ (Fig. 4b) (from Eq. 7) and using the slope of straight line portion for each sample, activation energy is estimated using $E_a = 2.303R \times$ slope. The variation of estimated activation energies with dopant concentration is shown in Fig. 4c. From the figure, it is clear that the activation energy decreases with increase of dopant concentration which indicates the reduction in average rate of collision (collision frequency) between polymer chains and increase of thermal stability of the polymer due to the addition of dopant [22].

Dielectric studies

Using the measured capacitance value, the dielectric constant has been estimated using the formula,

$$\epsilon_r = \frac{cd}{\epsilon_o l} \quad (8)$$

where c, d, ε_o and l represent capacitance, thickness of the sample, permittivity of free space (8.85×10^{-12} fm^{-1}) and area of the electrodes, respectively. Dielectric loss is calculated using the relation,

$$\epsilon^{\}} = \epsilon_r tan\delta \quad (9)$$

where $tan\delta$ is the measured dielectric loss tangent. Figure 5 a and b show the variation of dielectric constant and dielectric loss as a function of frequency for pure as well as doped polymer electrolytes at room temperature. Figure depicts that both the dielectric parameters show higher value at lower frequency [9] and the observed high dielectric constant value (Fig. 5a) is attributed to the electrode as well as space charge polarizations which are in accordance with non-Debye theory. According to this theory in a dielectric medium at low frequency, more number of charge carriers line up at the electrode/electrolyte interface due to sufficient time availability under slower variation of the applied field. The high dielectric loss (Fig. 5b) is because the oscillation of charge carriers as well as polar groups of the polymer with the applied field leads to loss of energy in the form of heat by internal friction. Both the dielectric parameters increase with dopant concentration and at 7.5 wt% the polymer electrolyte exhibited maximum dielectric property. This variation is mainly due to the increase in number of free charge carriers as well as number of dipoles due to polarization. Here, one can think of two types of dipoles that originate in polymer electrolytes.

First one is the creation of cation-anion pairs due to the dissociation of dopant and second one will be from polar groups of localized molecules within the polymer chains. These dipoles cannot cross the electrode/electrolyte interface due to the fact that thickness of polymer electrolyte is greater than hetero-charge layer at the interface [23]. On the other hand, they can reorient themselves via molecular motions associated with side chains of the polymer. The molecular fluctuations within the material results in high value of dielectric loss compared to dielectric constant. As the applied frequency increases, both dielectric constant and loss decreases continuously due to the dominant atomic as well as electronic polarizations and the space charge polarization decreases gradually. The observed frequency independent nature of the dielectric parameters at higher frequencies may be due to the fact that at higher frequencies, electric field variation is extremely high so that there is no excess ion diffusion in the direction of the field and the tendency of dipole to follow the field direction is less.

To understand the behavior of charge carriers with different temperatures, the variation of dielectric parameters has been studied at different temperatures for 7.5 wt% dopant concentration and the same is shown in Fig. 5c, d. From the figure, it is evident that both the dielectric constant and loss possesses higher values at lower frequency and increases with increase of temperature. As temperature increases, flexibility of the polymer chains increase due to the dissolution of crystalline phase of the polymer into amorphous matrix [24] as a result of the dielectric property increases with temperature. Also, more amount of salt dissociates into the polymer electrolyte which leads to increase of free motion of charge carriers and the dipoles can easily polarize in the direction of applied field at electrode-electrolyte interface. Hence, the space charge and dipole polarizations increase with temperature. As frequency increases, dipoles are unable to follow the field variation and the space charge effect of charge carriers tends to zero, as a result both dielectric constant and loss becomes frequency independent at higher frequencies [25].

Conductance spectra analysis

Using the estimated dielectric constant, ac conductivity of pure and doped PVA electrolyte has been estimated using the formula,

$$\sigma_{ac} = 2\pi f \varepsilon_o \varepsilon_r tan\delta \quad (10)$$

where f is the applied frequency. The variation of ionic conductivity with frequency for pure and doped polymer electrolytes is shown in Fig. 6a. From the figure, it is clear that conductivity of pure PVA increases with frequency which may be due to the fact that the groups within the polymer rotates with frequency and results into increase of flexibility of the bonds (contain flexible polar groups) [26]. In the doped
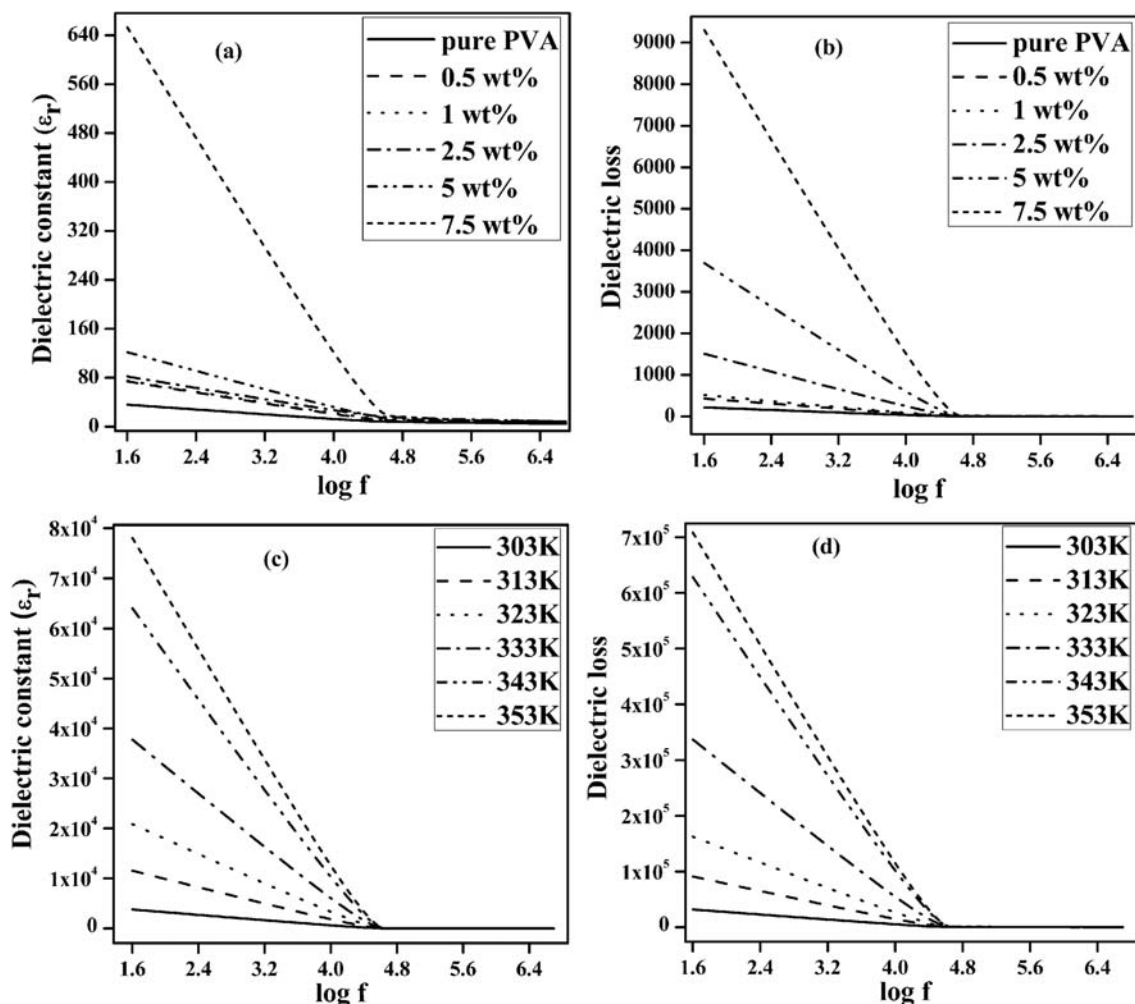
Fig. 5 **a** Variation of dielectric constant with frequency and **b** variation of dielectric loss with frequency, for pure PVA and NH$_4$Cl/PVA electrolytes. **c** Variation of dielectric constant with frequency and **d** variation of dielectric loss with frequency, for 7.5 wt% NH$_4$Cl/PVA electrolyte at different temperatures

polymer, electrolytes the dopant changes the structural and chemical composition of polymer and thus creates complexes within the polymer (as noticed in FTIR results). These complexes make the polymer chains more flexible and provide conducting pathways for charge carriers and hence the ionic conductivity increases with increase of dopant concentration

[27]. In the present study, the maximum ionic conductivity of 3.02×10^{-5} S/cm is observed for 7.5 wt% NH$_4$Cl-doped PVA electrolyte. Figure 6 a shows two distinct regions in the measured frequency range namely low-frequency plateau region (frequency independent) and high-frequency dispersion region (frequency dependent). The low-frequency region
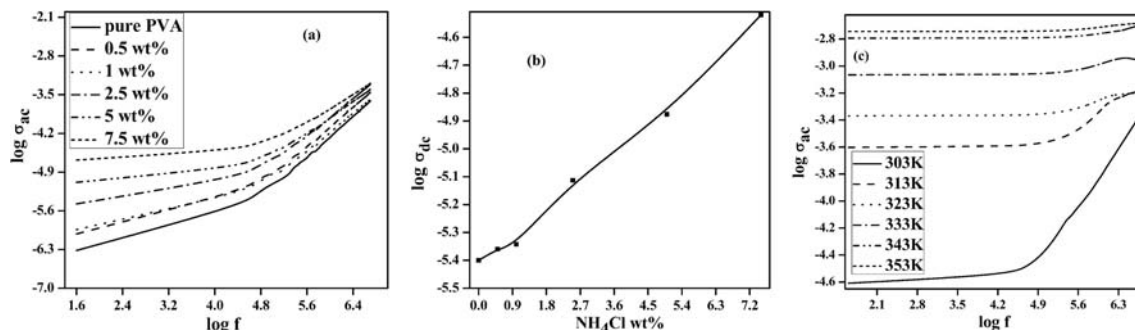

Fig. 6 **a** Variation of ac conductivity with frequency of pure PVA and NH$_4$Cl/PVA electrolytes. **b** Variation of ionic conductivity with NH$_4$Cl concentration. **c** Variation of ac conductivity of 7.5 wt% NH$_4$Cl/PVA electrolyte with frequency at different temperatures

describes the electrode/electrolyte interface phenomena which results into accumulation of charge carriers at the interface. In this region, mobility of charge carriers within the electrolyte is restricted and hence the ionic conductivity is low which is obtained by extrapolating the plateau region to zero frequency [28]. On the other hand at high-frequency region, the dissociation of charge carriers takes place within the electrolyte which enhances the mobility of charge carriers and increases the ionic conductivity with frequency.

Variation of ionic conductivity of pure and doped polymer electrolytes with dopant concentration at room temperature is shown in Fig. 6b. Figure shows that ionic conductivity increases with increase of dopant concentration. Here, the interaction of dopant with polymer forms the complexes (as observed in FTIR results) and high dispersion of H^+ ions takes place within the polymer electrolyte. Here, the formation of complexes reduces the barrier between trapping sites and helps the proton to hop from one site to another site through this conducting path. This corresponds to "Grotthus mechanism" of proton conduction. This mechanism depicts that in PVA/NH$_4$Cl electrolyte system proton conduction occurs through hopping in such a way that the loosely bound proton of NH$_4^+$ jumps from one site to another by creating vacancy in its initial site which will be filled by the neighboring proton. In this way, the charge transport takes place through the structure diffusion method following the Grotthus mechanism [29]. Due to this hopping, mobility of charge carriers increases which enhances ionic conductivity with dopant concentration.

The temperature dependence of conductivity of polymer electrolyte (7.5 wt% doped electrolyte) with frequency was carried out and the same is portrayed in Fig. 6c. From the Fig. 6c, it is noticed that the frequency-dependent conductivity response follows the Jonscher's Universal power law. Accordingly, total conductivity of the system can be expressed as

$$\sigma_{ac} = \sigma_{dc} + B\omega^s \qquad (11)$$

where σ_{dc} corresponds to dc conductivity, B indicates pre-exponential factor and s is temperature-dependent frequency exponent which explains the charge transport mechanism for conduction process within the electrolyte [30]. Figure 6 c shows that frequency-independent plateau region at low frequency corresponds to dc conductivity of the bulk material (listed in Table 5) followed by a high-frequency dispersion region (corresponding to ac conductivity) at all temperatures. The observed increase in ionic conductivity with temperature is due to the fact that, as temperature increases, the hydrostatic pressure between the atoms of polymer chains reduces thereby generating space around them and results into increased vibrational motion. The maximum dc conductivity obtained at 353 K is 1.81×10^{-3} S/cm which is about two orders higher than room temperature conductivity of the sample (7.5 wt% of dopant). From Fig. 6c, it is noticed that the hopping frequency (frequency at which the

Table 5 Temperature-dependent conductivity parameters

Temperature (K)	s	W_m (eV)	σ_{dc} (S/cm)
303	0.665	0.467	2.69×10^{-5}
313	0.248	0.215	2.53×10^{-4}
323	0.170	0.201	4.30×10^{-4}
333	0.097	0.190	8.66×10^{-4}
343	0.081	0.192	1.61×10^{-3}
353	0.063	0.194	1.81×10^{-3}

conductivity increases with faster rate) shifts to higher-frequency region with increase of temperature. This reflects the increase of ion hopping with temperature leading to increase in ionic conductivity at higher temperature. Using the slope of the curve at high-frequency region, the value of 's' at all temperatures is estimated and the same is given in Table 5. According to universal law, if the value of 's' is less than 0.7, the conduction mechanism follows correlated barrier hopping (CBH) model. If value of 's' lies between 0.7 and 1, the conduction mechanism belongs to quantum mechanical tunneling (QMT) model. From the Table 5, it is clear that the value of 's' varies from 0.665 to 0.063 with increase of temperature and indicates that in the present case, conduction mechanism follows the CBH model. According to this model, the ions are embedded by various potentials due to Coulomb repulsive force between them and hence the ions repose (reside) in a potential well. The increase of temperature leads to superposition of these potentials which will give strong potential to a single ion and thereby ion hopping occurs between localized sites. In this case, ion hopping can take place in two ways: one is ions that can undergo backward hopping to reach their initial site or can undergo forward hopping by creating a new potential. These hopping phenomena lead to increase in ionic mobility and hence they contribute to the total conductivity. Using the value of 's' energy required for the hopping of ions from one site to another (barrier height (W_m)) can be estimated using the formula [31],

$$W_m = \frac{6K_B T}{1 - S} \qquad (12)$$

where K_B is the Boltzmann constant and T is the absolute temperature. The calculated W_m values are listed in Table 5. From the table, it is noticed that W_m decreases initially (upto 333 K) and then increases with increase in temperature. So, here according to CBH model, two kinds of hopping process (backward and forward hopping) lead to increase of ionic conduction.

AC impedance analysis

Cole–Cole plot

Figure 7 a shows Cole–Cole plots of pure and doped polymer electrolyte at ambient temperature. The figure shows two
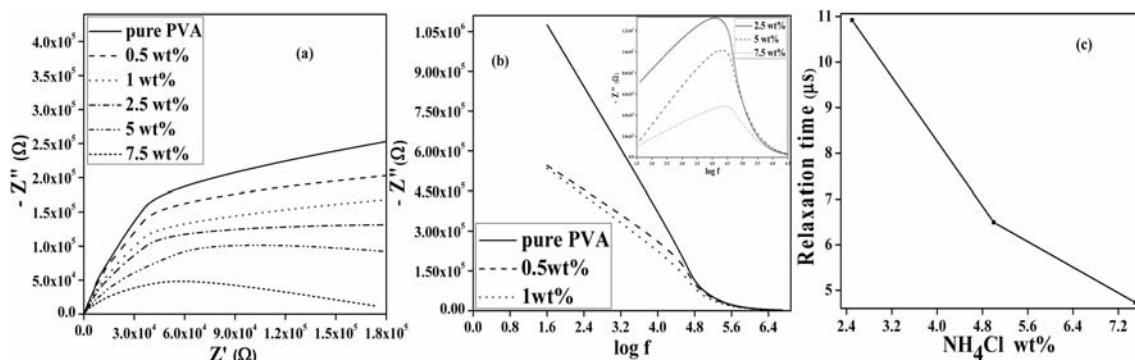
Fig. 7 **a** Cole–Cole plot of pure and NH$_4$Cl/PVA electrolytes. **b** Variation of imaginary part of impedance (Z″) with frequency for different NH$_4$Cl concentration in PVA. **c** Variation of relaxation time with NH$_4$Cl concentration

distinct regions: high-frequency oblique region (semicircle) and slanted portion at low frequency [32–37]. The oblique region corresponds to bulk conduction effect of polymer electrolyte because the mobility of charge carriers indicate non-Debye nature of relaxation and the linear region is attributed to non-homogeneity at electrode/sample interface [38, 39]. The semicircle arises because of the occurrence of two parallel phenomena within the polymer electrolytes such as charge carrier migration through vacant sites of polymer represented by resistor and polarization of immobile polymer chains in the alternating field represented by capacitor [40]. The low-frequency slanted line accounts for electrode/electrolyte interfacial phenomena and is inclined at an angle less than 90° (instead of appearing parallel to the imaginary axis as in the ideal case) which is due to roughness at the interface. In this study, it is noticed that the observed semicircle decreases with increase of dopant concentration and the slanted line bends towards Z′ axis. This variation suggests that the resistance for the ion transfer reduces and helps for conduction of ions within the electrolyte. As the dopant concentration increases, the number of mobile ions increases as a result ionic conductivity of the polymer electrolyte increases [41]. Similar behavior of ionic conductivity is reported by R. Hemalatha et al. [42] in NH$_4$Cl-doped PVA/amino acid proline electrolytes.

To understand the relaxation process of the conducting ion, relaxation time (τ) has been estimated using the plot of measured imaginary impedance with frequency for pure and doped polymer electrolytes (Fig. 7b). From the plot, the maximum peak (Fig. 7b inset) is observed which represents the relaxation frequency (f_{max}) [43]. Using the relaxation frequency, one can estimate the relaxation time by using the relation,

$$\tau = \frac{1}{\omega} \tag{13}$$

where $\omega = 2\pi f_{max}$ is the angular frequency.

From Fig. 7b, it is observed that for pure PVA and up to 1 wt% dopant concentrations, no relaxation peak is observed

which may be due to the fact that the relaxation peak lies below 40 Hz. From 2.5 wt% dopant concentration onwards, the relaxation peak is observed and its position shifts towards higher frequency with increase of dopant concentration, which indicates the reduction of relaxation process in the polymer electrolytes. The variation of relaxation time with dopant concentration is portrayed in Fig. 7c and it shows a decreasing trend in the relaxation time of the ions within the electrolytes which signifies the enhancement of intermolecular force between dopant and polymer chains [38, 44]. This leads to increase of ion hopping between the localized sites and hence ionic conductivity increases.

The impedance plot (Cole–Cole plot) of highest conducing (7.5 wt% NH$_4$Cl/PVA) polymer electrolyte at different temperatures is shown in Fig. 8a. From the figure, it is perceived that with increase of temperature, the observed semicircle (indicated as high-frequency region in Fig. 8a) decreases. The slopping line (indicated as low-frequency region in Fig. 8a, appeared as a spike) bends more toward imaginary axis with increase in temperature. This result indicates that the ionic resistance decreases to a very small value due to increase in flexibility of polymer chains which facilitate ion hopping within the polymer electrolytes [45]. So, the ionic mobility and hence the ionic conductivity increases with temperature. This enhancement of ionic conductivity may be due to the fact that PVA has an ability to dissociate more amount of salt into its matrix as compared to other polymers. Since the conductivity of the present polymer electrolyte is largely contributed by proton (smaller ionic radius), it can easily dissociate into the electrolyte and facilitate the increase of ionic mobility as well as conductivity.

The relaxation time of ions at different temperatures is determined using Fig. 8b and it is noticed that the relaxation frequency (f_{max}) shifts towards higher-frequency side with increase of temperature, and at higher temperatures, it becomes frequency independent. This shift of relaxation peak indicates the decrease of relaxation of ions within the electrolyte and signifies the non-Debye type of relaxation process [46].
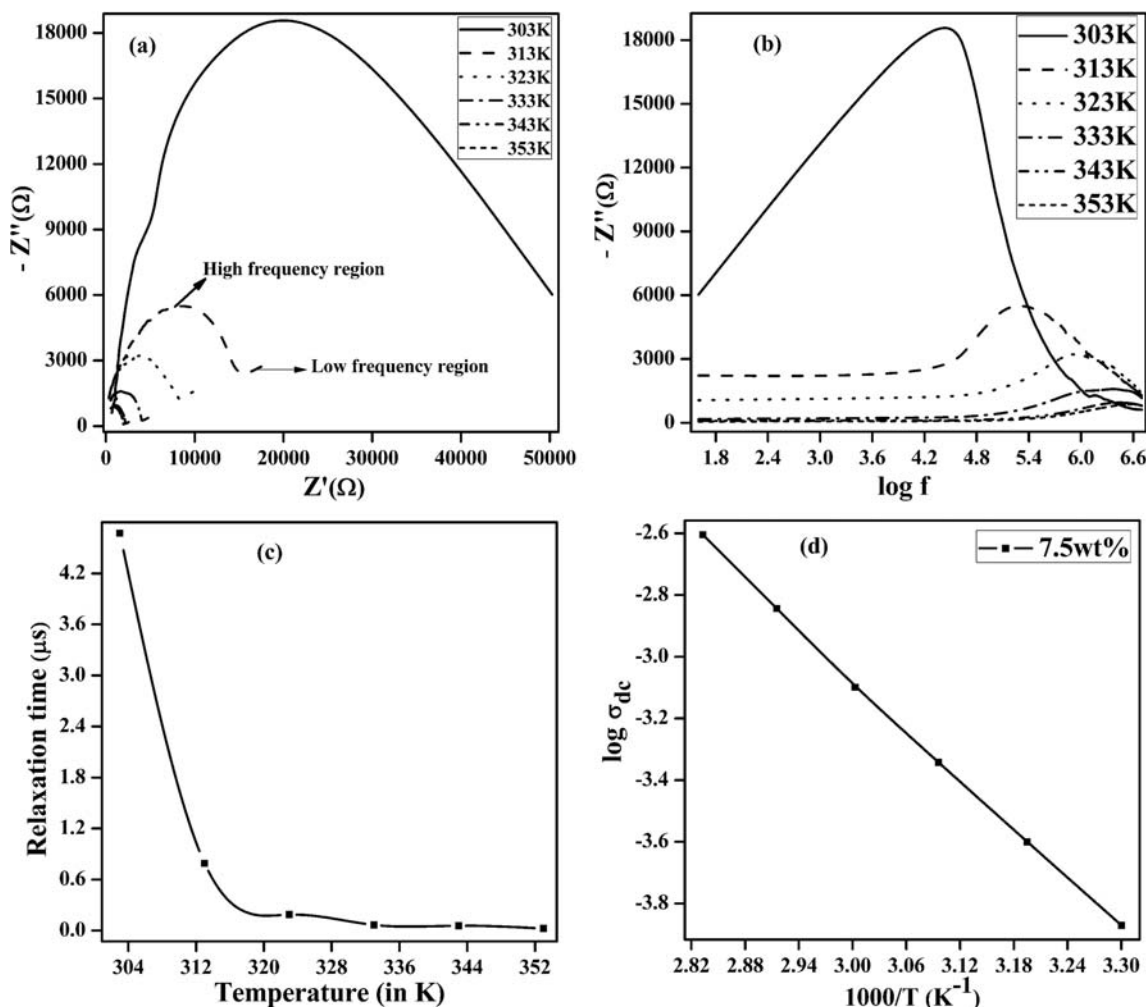
Fig. 8 **a** Cole–Cole plot of 7.5 wt% NH₄Cl/PVA polymer electrolyte at different temperatures. **b** Variation of imaginary part of impedance (Z'') with frequency of 7.5 wt% NH₄Cl/PVA electrolyte at different temperatures. **c** Variation of relaxation time of 7.5 wt% NH₄Cl/PVA electrolyte with temperature. **d** Temperature-dependent ionic conductivity of 7.5 wt% NH₄Cl/PVA electrolyte

Figure 8 c shows a sharp decrease in relaxation time of ions up to 315 K, and afterwards, it saturates with increase of temperature. This feature is mainly due to the fact that thermal energy up to 315 K increases the mobility of the polymer chains and facilitates the ion hopping between the localized sites and hence the reduction in τ took place; it results in increase of ionic conductivity.

Using the temperature-dependent conductivity, activation energy has been estimated using Arrhenius plot (Fig. 8d).

$$\sigma = \sigma_0 exp\left(\frac{-E_a}{K_B T}\right) \qquad (14)$$

Here, σ_o corresponds to the pre-exponential factor, K_B represents the Boltzmann constant, T is the absolute temperature and E_a is the activation energy. E_a is determined by the slope of Fig. 8d and is found to be 0.237 eV. This lower value of E_a signifies increase of amorphous phase of polymer electrolyte with increase of temperature; due to this, the ions become freely movable into the electrolyte via segmental motion of polymer

chains which results into faster internal modes. It also supports inter/intra chain ion hopping within the polymer electrolyte which results into increase of ionic conductivity [13, 31].

Transport properties

Charge carrier transport phenomena in polymer electrolytes depend on various factors such as degree of salt dissociation, ionic mobility and dielectric strength (dielectric constant). Using the Wagner's polarization technique, ion transport number has been determined in the highest conducting (7.5 wt% NH₄Cl-doped PVA) polymer electrolyte [47]. In this technique, the polymer electrolyte is sandwiched between two silver electrodes which form a cell and a constant dc voltage of 1.5 V is applied which is below the decomposition potential of the sample. Figure 9 a shows the variation of polarization current with time. Initial current that appeared is contributed by both ions as well as electrons and then spontaneous decay of current with time is observed. The decrease of current is

Fig. 9 **a** Variation of polarization current with time of 7.5 wt% NH$_4$Cl/PVA electrolyte at room temperature. **b** Variation of transient ionic current with time of 7.5 wt% NH$_4$Cl/PVA electrolyte
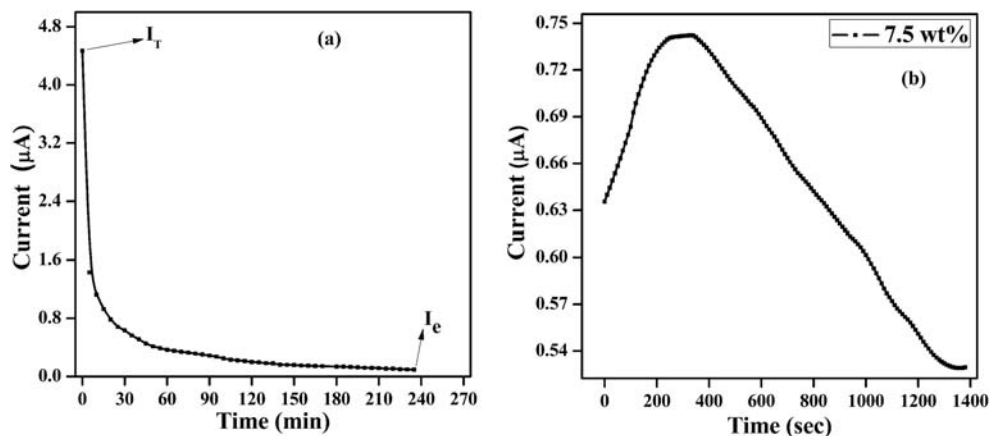
attributed to ionic (H$^+$) polarization. Once the H$^+$ ions get completely polarized, the current conduction in the electrolyte is due to electrons. Based on the data from Fig. 9a, the ion transport number has been calculated using the following relation [48],

$$t_+ = \frac{I_T - I_e}{I_T} = 1 - \frac{I_e}{I_T} \qquad (15)$$

where I_T is the total current, i.e. sum of ionic I_{ion} and electronic current I_e. Using this equation, the calculated ion transport number is 0.98. This indicates that the major charge transport has taken place due to ions and the electron contribution is very less which is about 0.02. The measured ion transport number is close to unity and hence this SPE is suitable for solid-state electrochemical application as suggested in the literatures [49, 50]. In order to determine the number of conducting ions in the electrolyte, transient ionic current (TIC) technique is followed. According to TIC technique after complete polarization of the cell, polarity of the applied potential is reversed and the current is recorded as a function of time. Here, on reversing the polarity, the H$^+$ ions collected at the negative electrode during polarization move to the other electrode. The observed TIC curve is shown in Fig. 9b. In the curve, a single current peak appeared indicates the presence of single ionic species in the electrolyte. The current peak gives the time of flight (t). Using this ionic mobility of the highest conducting polymer electrolyte has been determined by the relation,

$$\mu = \frac{d^2}{tv} \qquad (16)$$

where d is the thickness of the sample and v is the potential

applied. The calculated ionic mobility is 1.417×10^{-7} cm^2 V^{-1} S^{-1}.

Using the ionic mobility and ion transport number, the mobility of cation has been estimated using the equation,

$$\mu_+ = \mu t_+ \qquad (17)$$

where μ_+ and t_+ are the mobility and transport number of cation and the corresponding anion mobility is separated using the equation,

$$\mu_- = \mu - \mu_+ \qquad (18)$$

The calculated cation and anion mobilities are listed in Table 6. The diffusion coefficient of the ions in the polymer electrolyte has been obtained using following equation [51],

$$D = \frac{K_B T_a \, \sigma}{N e^2} \qquad (19)$$

where T_a is the ambient temperature, σ is the ionic conductivity of the polymer electrolyte, N is the number of charge carriers stoichiometrically related to composition of dopant, e is the charge of an electron. Hence, D is obtained to be 1.238×10^{-8} cm^2 S^{-1}.

Then,

$$D_+ = D t_+ \qquad (20)$$

where D_+ is the diffusion coefficient of cation.

Similarly, diffusion coefficient of anion (D_-) is given by

$$D_- = D - D_+ \qquad (21)$$

The calculated diffusion coefficients of cation and anion are listed in Table 6.

Table 6 Transport parameters of 7.5 wt% NH$_4$Cl/PVA electrolyte

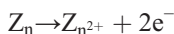| Weight ratio of PVA/NH$_4$Cl	N (cm^{-3})	t_+	t_-	μ_+ (cm^2 V^{-1} S^{-1})	μ_- (cm^2 V^{-1} S^{-1})	D_+ (cm^2 S^{-1})	D_- (cm^2 S^{-1})
92.5:7.5	3.974×10^{20}	0.98	0.02	1.389×10^{-7}	0.028×10^{-7}	1.213×10^{-8}	0.024×10^{-8}

From Table 6, it is clear that the highest conducting polymer electrolyte contains high cationic mobility (μ_+) and high cation diffusion coefficient (D_+) compared to anion which is because of more number of cations (H^+) transferred into the polymer electrolyte (in concordance with FTIR results). Here, it is attributed that more transfer of ions is facilitated due to pores formed on microstructure of the polymer electrolyte which is evident from AFM topographs and it enhances ionic conductivity.
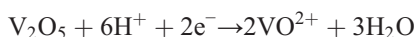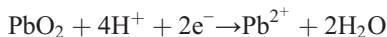
Proton battery characteristics

A proton battery is assembled with anode, proton-conducting SPE and cathode as discussed in experimental section. The schematic diagram of proton battery is given in Fig. 10a. The anode supplies protons to the battery electrolyte, and hence, $ZnSO_4 \cdot 7H_2O$ (among many metals, zinc is more superior) [52] is one of the components of anode. Based on conductivity analysis, the highest concentration of NH_4Cl (7.5 wt%)-doped polymer electrolyte exhibited maximum ionic conductivity and for this electrolyte the ion transport number has been found to be 0.98. So, this polymer electrolyte is used to fabricate proton battery. The chemical reactions which take place in this battery are given below,

Reaction at anode:

$$Z_n \rightarrow Z_{n^{2+}} + 2e^-$$

Reaction at cathode:

$$PbO_2 + 4H^+ + 2e^- \rightarrow Pb^{2+} + 2H_2O$$
$$V_2O_5 + 6H^+ + 2e^- \rightarrow 2VO^{2+} + 3H_2O$$

From the literature, oxidation and reduction potentials of Zn and PbO_2 are theoretically given by -0.7618 V and 1.455 V [12]. So, the theoretical open circuit voltage exhibited by overall reaction is $E_0 = 2.2168$ V. In the present work, the battery cell is fabricated in the form of $Zn/ZnSO_4 \cdot 7H_2O$/graphite powder ||7.5 wt% NH_4Cl/ PVA electrolyte || PbO_2/V_2O_5/graphite powder/polymer electrolyte which is given in Fig. 10a. This battery exhibited open circuit voltage of 0.567 V. This voltage is found to be lower than theoretically calculated voltage. The reduction in experimentally determined voltage compared to theoretical voltage may be due to the fact that, when the polymer electrolyte is sandwiched between cathode and anode, the reaction of the electrodes caused reduction of $ZnSO_4 \cdot 7H_2O$ at the anode in such a way that the zinc sulphate supplies protons which pass through the polymer electrolyte. The variation of open circuit voltage of the battery with time is shown in Fig. 10b. In the figure, it is observed that the open circuit voltage has been stabilized for about 1 month without any voltage drop. The proton batteries fabricated by pellet method have already been reported [12, 13, 51, 52]. But in the present work, the proton battery has been fabricated by slurry coating method. The advantages of this method over the pellet method are low cost, higher mechanical strength of the battery and longer duration of voltage sustainability. Hence, the battery has been stabilized for more days in open circuit condition compared to the previously reported proton batteries [13, 52].

The discharge characteristics of the proton battery are studied. For this, 1 MΩ load is applied to the battery and the variation of voltage with time is given in Fig. 10c. Figure 10 c depicts that when load is applied to the battery, there is sudden drop in voltage of the battery. The voltage drop may be due to the fact that before discharge, the battery was stabilized at open circuit condition (1 month duration). When higher load of 1 MΩ is applied to the battery, it causes displacement in actual voltage of the battery. The process is called as activation polarization and it takes place at the interface of polymer electrolyte and electrodes. After this state, the voltage of the battery remains constant as observed from the discharge curve (Fig. 10c). This region is known as plateau region. Then again, there is a drop in voltage with
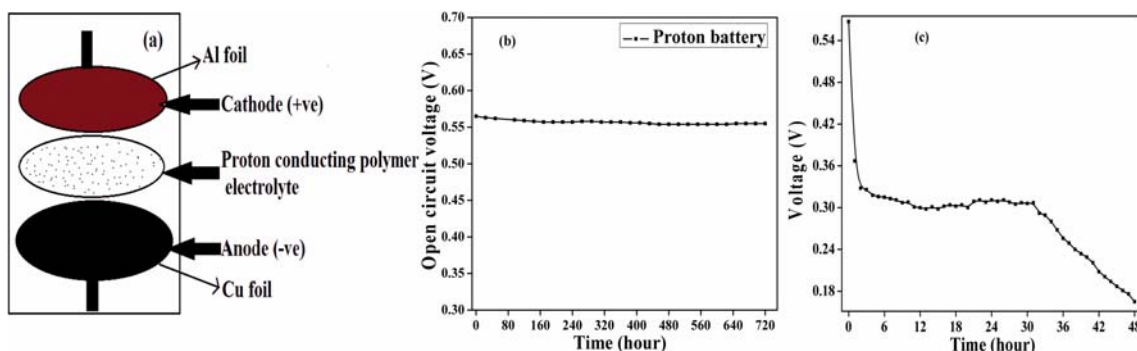

Fig. 10 a Schematic diagram of proton battery configuration. b Variation of open circuit voltage with time. c Discharge characteristics of proton battery at load resistance of 1 MΩ

Table 7 Parameters of proton battery

Cell parameter	
Open circuit voltage of the battery (V)	0.567
Area of the cell (cm^2)	15.12
Thickness of the cell (mm)	1
Weight of the cell (g)	2.03
Discharge time for plateau region (h)	30

respect to time. The observed battery parameters are listed in Table 7.

Conclusion

Proton conducting PVA/NH$_4$Cl SPEs with different concentrations of NH$_4$Cl have been prepared by solution casting method. FTIR results elucidate the polymer-salt complexation through inter/intra molecular hydrogen bonding. Increase of degree of crystallinity of the polymer electrolytes has been confirmed by XRD analysis. SEM image confirmed cluster formation of the dopant within the electrolyte. AFM topographs showed formation of pores in the polymer electrolytes which facilitate ionic mobility. TGA result indicates that the thermal stability of PVA has been improved by the addition of NH$_4$Cl. Dielectric studies revealed non-Debye nature of polymer electrolytes both at room temperature as well as at higher temperatures. Conductance spectra obeyed Jonscher's universal power law and exhibits CBH model of ionic conduction in polymer electrolytes. Impedance analysis revealed the decrease of relaxation time of ions with increase of dopant concentration as well as temperature. Ion transport number has been obtained to be 0.98. The proton battery fabricated using 7.5 wt% NH$_4$Cl/PVA electrolyte shows open circuit voltage of 0.567 V and the same voltage was sustained for about 1 month.

References

1. Kumar A, Logapperumal S, Sharma R, Das MK, Kar KK (2016) Li-ion transport, structural and thermal studies on lithium triflate and barium titanate incorporated poly (vinylidene fluoride-co-hexafluoropropene) based polymer electrolyte. Solid State Ionics 289:150–158. https://doi.org/10.1016/j.ssi.2016.03.008

2. Naga G, Vani S, Raja V, Sharma AK, Rao VVRN (2013) Development of PVP based polymer electrolytes for solid state battery applications. Int J Res Eng Adv Technol 1(3) ISSN: 2320–8791. https://www.researchgate.net/publication/317003139

3. Chew KW, Ng TC, How ZH (2013) Conductivity and microstructure study of PLA-based polymer electrolyte salted with Lithium Perchloride, LiClO4. Int J Electrochem Sci 8:6354–6364

4. Bamford D, Dlubek G, Reiche A, Alam MA, Meyer W, Galvosas P, Rittig F (2001) The local free volume, glass transition, and ionic conductivity in a polymer electrolyte: a positron lifetime study. J Chem Phys 115:7260. https://doi.org/10.1063/1.1402633

5. Rana P, Singh B, Chandra S (2006) Polymeric rechargeable solid-state proton battery. J Power Sources 161:702–706. https://doi.org/10.1016/j.jpowsour.2006.04.020

6. Agrawal RC, Hashmi SA, Pandey GP (2007) Electrochemical cell performance studies on all-solid-state battery using nano-composite polymer electrolyte membrane. Ionics 13:295–298. https://doi.org/10.1007/s11581-007-0112-0

7. Hema M, Selvasekerapandian S, Hirankumar G (2009) A. Sakunthala, D. Arunkumar, H. Nithya, structural and thermal studies of PVA:NH4I. J Phys Chem Solids 70:1098–1103. https://doi.org/10.1016/j.jpcs.2009.06.005

8. Ahmad NH, Isa MIN (2015) Structural and ionic conductivity studies of CMC based polymer electrolyte doped with NH4Cl. Adv Mater Res ISSN: 1662-8985 1107:247–252. https://doi.org/10.4028/www.scientific.net/AMR.1107.247

9. Radha KP, Selvasekarapandian S, Karthikeyan S, Hema M, Sanjeeviraja C (2013) Synthesis and impedance analysis of proton-conducting polymer electrolyte PVA:NH4F. Ionics 19:1437–1447. https://doi.org/10.1007/s11581-013-0866-5

10. Manjunath A, Deepa T, Supreetha NK, Irfan M (2015) Studies on AC electrical conductivity and dielectric properties of PVA/NH4NO3 solid polymer electrolyte films. Adv Mater Phys Chem 5:295–301. https://doi.org/10.4236/ampc.2015.58029

11. Praveena SD, Ravindrachary V, Bhajantri RF, Ismayil (2016) Dopant-induced microstructural, optical, and electrical properties of TiO2/PVA composite. Polym Compos 37:987–997. https://doi.org/10.1002/pc.23258

12. Vinoth Pandi D, Selvasekarapandian S, Bhuvaneswari R, Premalatha M, Monisha S, Arunkumar D, Junichi K (2016) Development and characterization of proton conducting polymer electrolyte based on PVA, amino acid glycine and NH4SCN. Solid State Ionics 298:15–22. https://doi.org/10.1016/j.ssi.2016.10.016

13. Sikkanthar S, Karthikeyan S, Selvasekarapandian S, Arunkumar D, Nithya H, Junichi K (2016) Structural, electrical conductivity, and transport analysis of PAN–NH4Cl polymer electrolyte system. Ionics 22:1085–1094. https://doi.org/10.1007/s11581-016-1645-x

14. Bhajantri RF, Ravindrachary V, Harisha A, Crasta V, Nayak SP, Poojary B (2006) Microstructural studies on BaCl2 doped poly (vinyl alcohol). Polymer 47:3591–3598. https://doi.org/10.1016/j.polymer.2006.03.054

15. Hari-Bala, Guo Y, Xu Z, Zhao J, Wuyou F, Ding X, Jiang Y, Yu K, Lv X, Wang Z (2006) Controlling the particle size of nanocrystalline titania via a thermal dissociation of substrates with ammonium chloride. Mater Lett 60:494–498. https://doi.org/10.1016/j.matlet.2005.09.030

16. Fernandes DM, Aiation A, Winkler H, Job AE, Radovanocic E, Gomez Pineda EA (2006) Thermal and photochemical stability of poly (vinyl alcohol)/modified lignin blends. Polym Degrad Stab 91:1192–1201. https://doi.org/10.1016/j.polymdegradstab.2005.05.024

17. Kesavana K, Mathewa CM, Rajendrana S, Ulaganathan M (2014) Preparation and characterization of novel solid polymer blend electrolytes based on poly (vinyl pyrrolidone) with various

concentrations of lithium perchlorate. Mater Sci Eng B 184:26–33. https://doi.org/10.1016/j.mseb.2014.01.009

18. Ramaraj B, Jaisankar SN (2008) Thermal and morphological properties of poly (vinyl alcohol) and layered double hydroxide (LDH) Nanocomposites. Polym-Plast Technol Eng 47:733–738. https://doi.org/10.1080/03602550802059170

19. G. Attia, M.F.H. Abd El-kader, Structural (2013) Optical and thermal characterization of PVA/2HEC Polyblend films. Int J Electrochem Sci 8:5672–5687

20. Abdelrazek EM, Elashmawi IS (2008) Characterization and physical properties of $CoCl_2$ filled polyethyl methacrylate films. Polym Compos 29:1036–1043. https://doi.org/10.1002/pc.20481

21. Coats AW, Redfern JP (1984) Kinetic parameters from Thermogravimetric data. Nature 201:681. https://doi.org/10.1038/201068a0

22. Abdelaziz M (2011) Cerium (III) doping effects on optical and thermal properties of PVA films. Physica B 406:1300–1307. https://doi.org/10.1016/j.physb.2011.01.021

23. Sai Prasanna CM, Austin Suthanthiraraj S (2017) Dielectric, thermal, and electrochemical properties of PVC/PEMA blended polymer electrolytes complexed with zinc triflate salt. Ionics 23:3137–3150. https://doi.org/10.1007/s11581-017-2109-7

24. Kalim D, Basheer Ahamed M, Polu AR, Sadasivuni KK, Khadheer Pasha SK, Ponnamma D, AlMaadeed MA-A, Deshmukh RR, Chidambaram K (2016) Impedance spectroscopy, ionic conductivity and dielectric studies of new li^+ ion conducting polymer blend electrolytes based on biodegradable polymers for solid state battery applications. J Mater Sci Mater Electron 27:11410–11424. https://doi.org/10.1007/s10854-016-5267-x

25. Vidyashree H, Bhajantri RF, Naik J (2017) Physico-chemical properties of bismuth nitrate filled PVA–$LiClO_4$ polymer composites for energy storage application. J Mater Sci Mater Electron 28:5827–5839. https://doi.org/10.1007/s10854-016-6254-y

26. Shreedatta H, Ravindrachary V, Praveena SD, Guruswamy B, Sagar RN (2018) Optical and Dielectric Properties of Li^+ ion conducting solid polymer electrolyte. Ind J Adv Chem Sci 6(2):83–87. https://doi.org/10.22607/IJACS.2018.602004

27. Mahendia S, Goyal PK, Tomar AK, Chahal RP, Kumar S (2016) Study of dielectric behavior and charge conduction mechanism of poly(Vinyl Alcohol) (PVA)-Copper (Cu) and gold (Au) nanocomposites as a bio-resorbable material for organic electronics. J Electron Mater 45(10). https://doi.org/10.1007/s11664-016-4677-0

28. Ragab HM (2011) Spectroscopic investigations and electrical properties of PVA/PVP blend filled with different concentrations of nickel chloride. Physica B 406:3759–3767. https://doi.org/10.1016/j.physb.2010.11.030

29. Buraidah MH, Teo LP, Majid SR, Arof AK (2009) Ionic conductivity by correlated barrier hopping in NH_4I doped chitosan solid electrolyte. Physica B 404:1373–1379. https://doi.org/10.1016/j.physb.2008.12.027

30. Tahalyania J, Rahangdalea KK, Aepurua R, Balasubramanian K, Datar S (2016) Dielectric investigation of conducting fibrous nonwoven porous mat fabricated by one-step facile electrospinning process. RSC Adv 6:36588. https://doi.org/10.1039/C5RA23012H

31. Ben Taher Y, Oueslati A, Maaloul NK, Khirouni K, Gargouri M (2015) Conductivity study and correlated barrier hopping (CBH) conduction mechanism in diphosphate compound. Appl Phys A Mater Sci Process 120:1537–1543. https://doi.org/10.1007/s00339-015-9353-3

32. Rathod SG, Bhajantri RF, Ravindrachary V, Naik J, Madhu Kumar DJ (2016) High mechanical and pressure sensitive dielectric properties of Graphene oxide doped PVA Nanocomposites. RSC Adv 6:77977–77986. https://doi.org/10.1039/C6RA16026C

33. Bi L, Shafi SP, Da'as EH, Traversa E (2018) Tailoring the cathode–electrolyte Interface with nanoparticles for boosting the solid oxide fuel cell performance of chemically stable proton-conducting

electrolytes. Small 14:1801231. https://doi.org/10.1002/smll.201801231

34. Ma J, Tao Z, Kou H, Fronzi M, Bi L (2019) Evaluating the effect of Pr-doping on the performance of strontium-doped lanthanum ferrite cathodes for protonic SOFCs. Ceram Int. https://doi.org/10.1016/j.ceramint.2019.10.017

35. Xu X, Wang H, Jinming M, Liu W, Wang X, Fronzi M, Bi L (2019) Impressive performance of proton-conducting solid oxide fuel cells using a first-generation cathode with tailored cations. J Mater Chem A 7:18792–18798. https://doi.org/10.1039/C9TA06676D

36. Xia Y, Jin Z, Wang H, Zheng G, Lv H, Peng R, Liu W, Bi L (2019) A novel cobalt-free cathode with triple-conduction for proton-conducting solid oxide fuel cells with unprecedented performance. J Mater Chem A 7:16136–16148. https://doi.org/10.1039/c9ta02449b

37. Xu X, Lei B, Zhao XS (2018) Highly-conductive proton-conducting electrolyte membranes with a low sintering temperature for solid oxide fuel cells. J Membr Sci 558:17–25. https://doi.org/10.1016/j.memsci.2018.04.037

38. Krishna Kumar V, Shanmugam G (2012) Electrical and optical properties of pure and Pb2+ ion doped PVA−PEG polymer composite electrolyte films. Ionics 18:403–411. https://doi.org/10.1007/s11581-011-0643-2

39. Du JF, Bai Y, Chu WY, Qiao LJ (2010) Synthesis and performance of proton ConductingChitosan/NH4Cl electrolyte. J Polym Sci B Polym Phys 48:260–266. https://doi.org/10.1002/polb.21866

40. Shreedatta H, Ravindrachary V, Praveena SD, Guruswamy B, Sagar RN, Sanjeev G (2018) Relaxation and transport properties of li^+ conducting biocompatible material for battery application. Ion AIP Conf Proc 1942:110043. https://doi.org/10.1063/1.5029026

41. Nadimicherla R, Sharma AK, Narasimha Rao VVR, Chen W (2014) AC conduction mechanism and battery discharge characteristics of (PVC/PEO) polyblend films complexed with potassium chloride. Measurement 47:33–41. https://doi.org/10.1016/j.measurement.2013.08.047

42. Hemalatha R, Alagar M, Selvasekarapandian S, Sundaresan B, Moniha V, Boopathi G, Christopher Selvin P (2019) Preparation and characterization of proton-conducting polymer electrolyte based on PVA, amino acidproline, and NH4Cl and its applications to electrochemical devices. Ionics 25:141–154. https://doi.org/10.1007/s11581-018-2564-9

43. Kathayat K, Panigrahi A, Pandey A, Kar S (2012) Characterization of electrical behavior of $Ba_5HoTi_3V_7O_{30}$ ceramic using impedance analysis. Mater Sci Appl 3:390–397. https://doi.org/10.4236/msa.2012.36056

44. Chawla M, Shekhawat N, Aggarwa S, Sharma A, Nair KGM (2014) Cole-cole analysis and electrical conduction mechanism of N^+ implanted polycarbonate. J Appl Phys 115:184104. https://doi.org/10.1063/1.4876123

45. Saroj AL, Singh RK (2012) Thermal, dielectric and conductivity studies on PVA/ionic liquid [EMIM][$EtSO_4$] based polymer electrolytes. J Phys Chem Solids 73:162–168. https://doi.org/10.1016/j.jpcs.2011.11.012

46. Sahoo PS, Panigrahi A, Patri SK, Choudhary RNP (2009) Structural and impedance properties of Ba_5 $DyTi_3V_7O_{30}$. J Mater Sci Mater Electron 20:565–570. https://doi.org/10.1007/s10854-008-9766-2

47. Wagner B, Wagner C (1957) Electrical conductivity measurements on cuprous halides. J Chem Phys 26:1597. https://doi.org/10.1063/1.1743590

48. Prajapati GK, Roshan R, Gupta PN (2010) Effect of plasticizer on ionic transport and dielectric properties of PVA–H_3PO_4 proton conducting polymeric electrolytes. J Phys Chem Solids 71:1717–1723. https://doi.org/10.1016/j.jpcs.2010.08.023

49. Bhavani S, Ravi M, Rao VVRN (2014) Studies on electrical properties of PVA: NiBr₂ complexed polymer electrolyte films for battery applications. Int J Eng Sci Innov Technol 3(4) ISSN: 2319–5967

50. Anantha PS, Hariharan K (2005) Physical and ionic transport studies on poly (ethylene oxide)–NaNO₃ polymer electrolyte system. Solid State Ionics 176:155–162. https://doi.org/10.1016/j.ssi.2004.07.006

51. Leena Chandra MV, Karthikeyan S, Selvasekarapandian S, Vinoth Pandi D, Monisha S, Arulmozhi Packiaseeli S (2016) Characterization of high ionic conducting PVAc–PMMA blend-based polymer electrolyte for electrochemical applications. Ionics 22:2409–2420. https://doi.org/10.1007/s11581-016-1763-5

52. Sivadevi S, Selvasekarapandian S, Karthikeyan S, Sanjeeviraja C, Nithya H, Iwai Y, Kawamura J (2015) Proton-conducting polymer electrolyte based on PVA-PAN blend doped with ammonium thiocyanate. Ionics 21:1017–1029. https://doi.org/10.1007/s11581-014-1259-0